fluctuations. Some elements of these ideas were suggested over 20 years ago (*5*, *6*).

The model results are observable in the real world. For instance, SST patterns and their associated atmospheric patterns, as determined from observations (*1*, *2*, *4*), are close to those from our simulation. Further, projection of the last 45 years of observed SST fields onto the leading EOF of the anomalous SST field from the model yielded a principal component whose amplitude and characteristic time scale closely resemble those of the principal component of the model. More important, the relation between atmospheric response and ocean transport indices was the same in the model and in observations (*17*): Gyre strength and atmospheric pressure vary in phase on decadal time scales (Fig. 4).

North Atlantic SST variability exhibits pronounced energy at time scales of about 10 years (*18*). This pattern is consistent with our scenario, because the zonal width of the North Atlantic is only about half that of the North Pacific. Moreover, the spatial patterns of the decadal variability observed in the North Atlantic region agree with those we found in the North Pacific region: Anomalously warm SSTs and anomalously high pressure occur together and the associated changes in the surface heat flux and oceanic mixing tend to reinforce the SST anomalies (*18*).

Both the model and observations show a strong, simultaneous wintertime relation between low-pass filtered anomalies of atmospheric pressure in the heart of the main atmospheric response region south of the Aleutians (Fig. 3) and air temperature over North America (Fig. 5) (*1*, *4*, *19*). The remarkable accuracy of the model in reproducing the dipole correlation over North America suggests that it can be used to forecast decadal climate change numerically over North America (*20*). At a minimum, knowledge of the present phase of the Pacific mode obtained from current observational programs should allow a "nowcast" (*21*) of expected climate "bias" associated with this decadal climate change, which is equivalent to a climate forecast of several years in the future.

REFERENCES AND NOTES

1. J. Namias, *J. Geophys. Res.* **64**, 631 (1959); *Mon. Weather Rev.* **97**, 173 (1969).
2. N. E. Graham, *Clim. Dyn.* **10**, 135 (1994).
3. A. J. Miller *et al.*, *ibid.* **9**, 287 (1994).
4. K. E. Trenberth and J. W. Hurrell, *ibid.*, p. 303.
5. J. Bjerknes, *Advances in Geophysics* (Academic Press, New York, 1964), pp. 1–82.
6. W. B. White and T. P. Barnett, *J. Phys. Oceanogr.* **2**, 372 (1972).
7. G. A. Jacobs *et al.*, *Nature* **370**, 360 (1994).
8. M. Latif *et al.*, *Tellus A* **46**, 351 (1944). The atmospheric component is the standard Max-Planck-Institut (MPI) model ECHAM3, while the oceanic component is the Hamburg Ocean Model in Primitive Equations (HOPE) model, a primitive equation model of global ocean dynamics also developed at MPI. Both models have a resolution of approximately 2.5° by 2.5° in mid-latitudes. The resolution of the ocean model, however, is higher in the tropics. The ocean and atmosphere interact within the region from 60°N to 60°S, without the application of any flux correction. Poleward of 60°, SST and salinity are relaxed to the climatology by the use of a Newtonian formulation.
9. M. Latif, A. Sterl, E. Maier-Reimer, M. M. Junge, *J. Clim.* **6**, 700 (1993).
10. T. P. Barnett, *Mon. Weather Rev.* **111**, 756 (1983).
11. D. L. T. Anderson and A. E. Gill, *Deep Sea Res.* **22**, 583 (1975).
12. D. L. T. Anderson, K. Bryan, A. E. Gill, R. C. Pacanowski, *J. Geophys. Res.* **84**, 4795 (1979).
13. A. E. Gill, *Atmosphere-Ocean Dynamics* (Academic Press, New York, 1982), pp. 507–512.
14. T. N. Palmer and Z. Sun, *Q. J. R. Meteorol. Soc.* **111**, 947 (1985); N.-C. Lau and M. J. Nath, *J. Clim.* **3**, 965 (1990); Y. Kushnir and N.-C. Lau, *ibid.* **5**, 271 (1992); L. Ferranti, F. Molteni, T. N. Palmer, *Q. J. R. Meteorol. Soc.*, in press.
15. Typical decadal-scale 500-hPa height anomalies over the North Pacific simulated by the coupled model are on the order of about 10 geopotential meters.
16. J. D. Horel and J. M. Wallace, *Mon. Weather Rev.* **109**, 813 (1981).
17. The ocean transport index from the model is the meridional gradient of the density field in the upper 500 m at the dateline. An index of the Kuroshio strength (and, hence, the gyre) was taken to be the observed sea level at Hosojima, Kyushu, Japan.
18. C. Deser and M. L. Blackmon, *J. Clim.* **6**, 1743 (1993).
19. T. P. Barnett, *Mon. Weather Rev.* **109**, 1021 (1981).
20. The long-range (decadal) forecasts would require that the ocean component of the coupled model be initialized with at least the observed thermal structure of the upper 500 m of the Pacific over a region extending from the Aleutians to 20°N and from Asia to North America. Existing expendable bathythermograph and buoy programs are close to providing the required information.
21. This phrase was coined by J. J. O'Brien (Florida State University).
22. We thank D. Cayan and W. White for many fruitful discussions; N. Schneider and D. Pierce for providing suggestions on an earlier version of the manuscript; and T. Stockdale, J. Wolff, and E. Maier-Reimer for helping to develop the coupled model; we also thank the Theoretical Applications Division of the Los Alamos National Laboratory for making most of the computer time available for these runs; D. Poling for tending these runs and managing the extensive output files; and C. Keller for facilitating the cooperation on this project. In addition, we thank M. Junge, J. Ritchie, T. Tubbs, and M. Tyree for providing computational assistance. Supported in part by the National Science Foundation under grant NSFATM 9314495, the U.S. Department of Energy's CHAMP program under grant DE-FG03-91-ER61215 (T.P.B.), the German Climate Computer Center (DKRZ), and the European Community under grant EV5V-CT92-0121 (M.L.).

27 June 1994; accepted 30 August 1994

Middle Cambrian Arthropod Embryos with Blastomeres

Xi-guang Zhang and Brian R. Pratt

A phosphatized Middle Cambrian (~510 million years ago) fauna from Duyun, southern China, has yielded fossil embryos that may be of arthropod affinity and could belong to the co-occurring eodiscid trilobite *Pagetia* sp. The shell was most likely flexible and possessed at least two thin layers. Four embryos reveal blastomeres, and two embryonic stages are represented. These embryos demonstrate that the basic paradigm for the growth of the invertebrate embryo has not changed in more than half a billion years.

A unicellular zygote (fertilized egg) is converted into a multicellular organism by successive cleavages during embryonic development. Lacking mineralized tissues, however, invertebrate eggs are unlikely to escape breakdown. Fossil examples are therefore exceedingly scarce, and none reveal embryonic stages. Among the Echinodermata, for instance, only a single blastoid from the Lower Pennsylvanian of Oklahoma contains probable eggs (*1*). Fossil trilobite eggs were mentioned in several 19th-century publications but were not conclusive (*2*). The trilobite embryo and the suspected preprotaspis stage have been unknown (*3*). Possible ostracode eggs from the Lower Cambrian of China (*4*) and Lower Cretaceous of Brazil (*5*), as well as shrimp eggs similarly from the Cretaceous of Brazil (*6*), are nondescript spheres (*7*). Possible Middle Cretaceous insect eggs from Brazil (*8*) have not been substantiated, but a single, Upper Cretaceous moth eggshell from Massachusetts does possess a well-preserved lepidopteran sculpture (*9*). In this report, we describe fossil eggs that contain embryos bearing delicate blastomeres.

These embryos are phosphatized and co-occur with many trilobite juveniles (protaspides and meraspides) of the eodiscid *Pagetia* sp. and an unidentified polymeroid trilobite, a few adult bradoriid ostracodes, and lots of inarticulate brachiopod valves. We liberated these fossils by dilute (~5%) acetic acid digestion of 7 kg of a thin, bioclastic limestone bed sandwiched between gray dolomites within the lower part of the Middle Cambrian Gaotai Formation in Duyun, Guizhou, China.

The five embryos are ovoid (Figs. 1 and 2). The lengths range from 0.30 to 0.35 mm, and the widths from 0.24 to 0.27 mm (*10*). The shell, being about 1.5 μm thick and

---

Department of Geological Sciences, University of Saskatchewan, Saskatoon, Saskatchewan S7N 0W0, Canada.

seemingly composed of two layers (*11*), was probably slightly flexible in that it was evidently bent down (Fig. 1B) or pushed in (Fig. 1E) before lithification. Polygonal structures are visible beneath the shells of two embryos under reflected light: One has its entire surface under the shell fully occupied by about 60 tightly packed polygons (mainly hexagons with a few pentagons and heptagons) of varying size (Fig. 2B); the other only has a patch of the polygon pattern preserved. We interpret the polygonal structures as blastomeres comprising the blastoderm around the yolk. Under the scanning electron microscope (SEM), because of the obstruction of the shell, only where the outermost thin shell layer is partially flaked off do its surviving parts, defined in positive relief, roughly outline polygonal blastomeres beneath (Fig. 1, A and B, and Fig. 2A). In a third embryo (Fig. 1C), apatite (calcium phosphate) replaced polygonal blastomeres. The fourth embryo is broken (Fig. 1D), but where the shell is flaked off, polygonal holes also appear to outline blastomeres underneath. Although some of the cell walls are visible on the broken side, no recognizable structure is evident in the center of this embryo. Fine dimples on the exterior of a fifth embryo (Fig. 1E) may reflect some of the underlying blastomeres (*12*).

The number of blastomeres can be estimated from the average length of the sides of some well-defined polygons (*13*). Both the third and fourth embryos (Fig. 1, C and D) exhibit smaller polygons and thus contain about twice as many cleavage cells as each of the first two embryos (Fig. 1A). Presumably, they belong to two successive (64-cell and 128-cell) cleavage stages. Unfortunately, no evidence is available to ascertain if gastrulation had started.

In general, the ovoid shape of the five embryos, their flexible shells, tightly packed blastomeres, and cleavage stages are all typical embryonic phenomena among modern invertebrates. These embryos cannot be assigned unequivocally to a particular Middle Cambrian taxon. The embryo morphology, the cleavage cells, and possible cleavage stages do closely resemble those of extant arthropods more than those of any other invertebrate group (*14*, *15*). We therefore infer that these Middle Cambrian embryos have an arthropod affinity. Because the assemblage does not contain juvenile ostracodes, we suggest that populations of this group hatched and reached adulthood elsewhere in the sedimentary basin. On the other hand, coexisting eodiscid and polymeroid trilobite protaspides and meraspides are abundant, indicating that these trilobites did complete their life cycles in this depositional setting. Thus, the evidence is in favor of a trilobite affinity for these embryos (*16*). They more likely belong to the eodiscid *Pagetia* sp., on the basis of their size (*17*). However, we cannot rule out the possibility that they might belong to a soft-bodied arthropod whose later instars were not preserved.

Early replacement of soft tissues by apatite before substantial degradation is probably the most important taphonomic means by which soft bodies and even cellular details of tissues can be fossilized (*6*, *18*). The fossilization of these embryos at certain stages indicate that they died during their initial development and were almost immediately replaced by apatite. However, we do

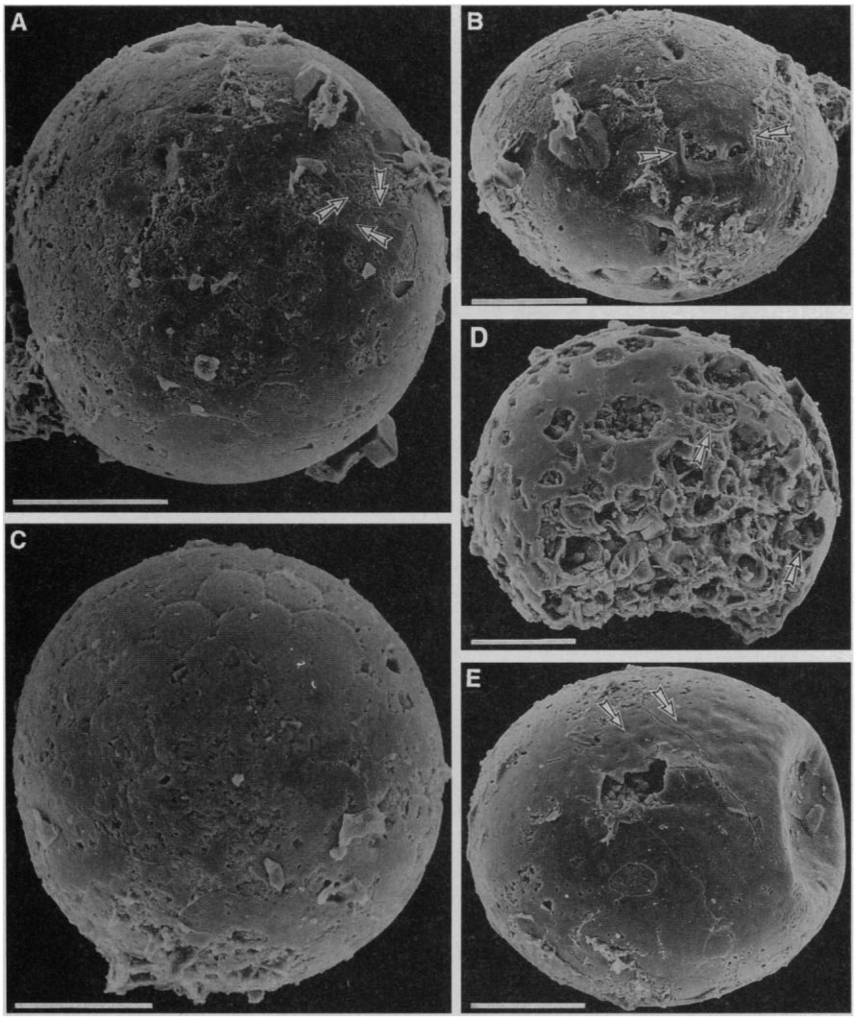

Fig. 1. Phosphatized (possibly eodiscid trilobite) embryos from the Middle Cambrian Gaotai Formation in Duyun, Guizhou, southern China. **(A)** A complete embryo (Specimen CIGM-DY 0002 deposited in the Chengdu Institute of Geology and Mineral Resources, Chengdu, China) with blastomeres, of which only a few are defined by polygons of surviving parts of the outermost thin shell layer (arrows indicate three adjacent sides shared by three polygons). **(B)** Different view of the embryo in (A) showing other polygons (arrows indicate opposite sides of a polygon). The shell is bent down beside a crack at the lower left side. **(C)** An incomplete embryo (CIGM-DY 0003) whose other half opposite this surface has broken off. Part of its shell is missing so that some blastomeres beneath are visible. **(D)** A broken embryo (CIGM-DY 0004) whose blastomeres are visible (arrows indicate surviving normal walls of polygonal cells). **(E)** An entire embryo (CIGM-DY 0001) with its shell caved in on the right side and partially ornamented with fine depressions on the outer surface (arrowed). Scale bars, 0.1 mm.

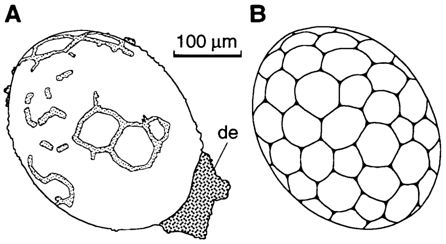

Fig. 2. Drawings of a Middle Cambrian arthropod (possibly eodiscid trilobite) embryo with blastomeres, based on the specimen in Fig. 1, A and B (CIGM-DY 0002). **(A)** Sketch showing the surviving outermost thin layer of the shell (fine dotted areas) corresponding to the blastomeres beneath. Minute debris fixed on the shell labeled as "de." **(B)** Reconstruction of the same embryo.

not understand why this early apatite mineralization seemingly affected so few embryos, despite the multitudes probably laid, and did not lead to any soft tissue preservation for other fossils even though there was widespread phosphatization of calcitic skeletons in the Duyun fauna. These embryos preserve no obvious microbes, so we cannot ascertain whether bacterial activity was involved in the phosphatization process, as has been suggested (*6*, *18*, *19*).

REFERENCES AND NOTES

1. S. G. Katz and J. Sprinkle, *Science* **192**, 1137 (1976).
2. J. Barrande, *Système Silurien du Centre de la Bohême lère Partie: Recherches Paléontologiques*, vol. 1 of *Crustacés, Trilobites* (self-published, Prague and Paris, 1852); C. E. Beecher, *Am. Geol.* **16**, 166 (1895).
3. S. E. Speyer and B. D. E. Chatterton, *Hist. Biol.* **3**, 27 (1989).
4. X.-G. Zhang, *Alcheringa* **11**, 1 (1987).
5. R. H. Bate, *Palaeontology* **15**, 379 (1972).
6. D. E. G. Briggs, A. J. Kear, D. M. Martill, P. R. Wilby, *J. Geol. Soc. London* **150**, 1035 (1993).
7. Cambrian spheres *Archaeooides* and *Olivooides* found from several localities in China were all described as fossils of uncertain systematic position because of their simple, nondiagnostic morphology. Some of them are oval-shaped [X. Yang, Y. He, S. Deng, *Bull. Chengdu Inst. Geol. Mineral. Resour. Chinese Acad. Geol. Sci.* **4**, 91 (1983); P. Chen, *Prof. Pap. Strat. Palaeontol.* **13**, 49 (1984)] and may be eggshells, but published illustrations are insufficient to demonstrate this.
8. M. da S. P. Regali and W. A. S. Sarjeant, *Micropaleontology* **32**, 163 (1986).
9. L. F. Gall and B. H. Tiffney, *Science* **219**, 507 (1983).
10. Egg size and morphology may vary within genera and species of some living crustaceans [G. Mura, *Crustaceana* **61**, 241 (1991); *ibid.* **63**, 225 (1992)] and chelicerates (*14*).
11. The thickness of the shell is measurable in three of the eggs under a SEM. An outermost layer, 0.5 μm thick, is determined in three eggs (Fig. 1, A, B, C, and E).
12. Dimples on part of the surface of the fifth embryo resemble those on the blastomeres of extant crayfish embryos [J. D. Celada, P. de Paz, V. R. Gaudioso, R. Fernández, *Anat. Rec.* **219**, 304 (1987); J. D. Celada, J. M. Carral, J. González, *Crustaceana* **61**, 225 (1991)] and may reflect partial collapse of these cells.
13. During the embryonic process, the surface area of an embryo can be considered as a constant even though the number of blastomeres increases with growth. Considering, in the simplest case, polygons on the outer surface of a shell to be all hexagons, the surface area (A) of the embryo is
$$A = \frac{3\sqrt{3}}{2}(s_1^2 + s_2^2 + \ldots + s_n^2) \approx \frac{3\sqrt{3}}{2} nS^2$$
where s is the length of a side of a hexagon, S is the average length of all measured sides, and n is the total number of hexagons. Therefore, for any two embryos, their equal surface areas can roughly be expressed as
$$\frac{3\sqrt{3}}{2} n_1 S_1^2 = \frac{3\sqrt{3}}{2} n_2 S_2^2$$
or $n_1/n_2 = S_2^2/S_1^2$. If the number of blastomeres would double in the subsequent division stage (that is, $n_1/n_2 = 2$) then $S_1/S_2 = \sqrt{2}/2$. The average length S_1 of the third embryo is about 0.008 mm, and S_2 for the first two embryos showing blastomeres is 0.011 mm; $S_1/S_2 \approx 0.7 \approx \sqrt{2}/2$.
14. K. Sekiguchi, Y. Yamamichi, H. Seshimo, H. Sugita, in *Biology of Horseshoe Crabs*, K. Sekiguchi, Ed. (Science House, Tokyo, 1988), pp. 133–224.
15. D. T. Anderson, in *Arthropod Phylogeny*, A. P. Gupta, Ed. (Van Nostrand Reinhold, New York, 1979), pp. 59–105; R. Nagabhushanam and R. Sarojini, *Invertebrate Embryology* (Oxford, New Delhi, 1985).
16. Trilobita are closely related to Crustacea and Chelicerata [D. E. G. Briggs and R. A. Fortey, *Science* **246**, 241 (1989); G. Budd, *Nature* **364**, 709 (1993)]. The four fossil embryos exhibiting blastomeres are much smaller than, but otherwise appear comparable to, stage 2 and stage 3 embryos of modern horseshoe crabs (*14*), and their shells are similarly laminated.
17. Of the associated youngest trilobite instars, the protaspis of the unidentified polymeroid trilobite is about 0.50 mm long and wide, whereas the protaspis of *Pagetia* sp. is about 0.25 mm in our collection and 0.28 to 0.35 mm in previously reported specimens [J. H. Shergold, *Alcheringa* **15**, 65 (1991)]. On the basis of size, the five embryos are more likely those of an eodiscid trilobite.
18. D. M. Martill, *Nature* **346**, 171 (1990); D. E. G. Briggs and A. J. Kear, *Science* **259**, 1439 (1993).
19. D. M. Martill, *Palaeontology* **31**, 1 (1988); P. A. Allison, *Paleobiology* **14**, 331 (1988).
20. This work was supported by the Natural Sciences and Engineering Research Council of Canada. We thank D. M. Lehmkuhl and D. M. Martill for criticizing an earlier version of the manuscript and Y. Yano for assistance with SEM photography.

7 June 1994; accepted 30 August 1994

Role of Oocyte Position in Establishment of Anterior-Posterior Polarity in *Drosophila*

Acaimo González-Reyes and Daniel St Johnston*

The polarized microtubule cytoskeleton of the *Drosophila* oocyte directs the localization of the maternal determinants which establish the anterior-posterior (AP) axis of the embryo. Because the formation of this microtubule array is dependent on signals from the follicle cells that surround the oocyte, it has been proposed that AP polarity originates in the follicle cells. Here it is shown that the movement of the oocyte to the posterior of the egg chamber early in oogenesis determines AP polarity in the follicle cell layer, and also in the oocyte. Moreover, the generation of AP asymmetry requires signaling from the germ line to the soma and back again.

The AP axis of the *Drosophila* embryo is defined during oogenesis by the localization of the maternal determinants bicoid and oskar mRNAs to opposite poles of the oocyte (*1*–*4*). When these transcripts first localize, the oocyte cytoskeleton shows clear AP asymmetry: The microtubule-nucleating activity lies at the anterior of the cell, and the plus ends of the microtubules extend toward the posterior pole (*5*, *6*). Because the transport and anchoring of bicoid and oskar mRNAs is microtubule dependent (*6*, *7*), AP polarity within the oocyte is defined by the organization of the cytoskeleton. The formation of this polarized microtubule array depends, at least in part, on signals from the somatic follicle cells that surround the germline cyst (15 nurse cells and the oocyte), because the removal of *Notch* or *Delta* function in the follicle cells generates two anterior poles within the oocyte (*8*). This result led to the proposal that AP polarity originates in the follicle cells (*9*). Because the first visible asymmetry in egg chamber development is the movement of the oocyte to the posterior of the germline cyst (Fig. 1A), an alternative possibility is that AP polarity arises with this movement. To investigate whether the placement of the oocyte at the posterior plays a role in axis formation, we examined the consequences of changes in oocyte position on the determination of follicle cell fates and on the development of AP polarity. To do this, we took advantage of mutations at the *spindle*-C locus (*spn-C*)(*10*), a maternal effect gene that is required for the correct positioning of the oocyte early in oogenesis. In ~60% of *spindle-C*^{094} mutant egg chambers, the oocyte fails to move to the posterior and lies either at the anterior of the germline cyst or in the middle, with nurse cells on both sides (bipolar) (Fig. 1B) (*11*). This phenotype has also been described for *dicephalic* mutants (*12*).

In a wild-type egg chamber, follicle cell behavior shows several AP asymmetries (*13*). During stage 9 of oogenesis (*14*), most of the follicle cells migrate posteriorly over the nurse cells to form a columnar layer that surrounds the oocyte (Fig. 2A). Shortly thereafter, 6 to 10 follicle cells at the anterior tip of the egg chamber (the border cells) migrate between the nurse cells to reach the anterior of the oocyte. Once the columnar follicle cells have covered the exterior of the oocyte, the most anterior of these cells migrate centripetally to separate the oocyte from the nurse cells (Fig. 2C). Both the border cells and the centripetal follicle cells express a gene called *slow border cells* [*slbo* (*15*)] and eventually collaborate to produce the micropyle, an anterior structure of the egg shell (Fig. 2E). In bipo-

---

The Wellcome/CRC Institute and Department of Genetics, University of Cambridge, Cambridge CB2 1QR, England.

*To whom correspondence should be addressed.